



Computational Design and Static-structural Analysis of a Small-scale Turbojet Propulsive Engine for an Unmanned Aerial Vehicle

Samuel O. Effiom¹, Fidelis I. Abam², Burhan Saeed³, Sunday O. Ochedi¹, John E. Evareh^{1,*}

¹Applied Energy and Propulsion Engineering Research Group (AEPERG), Department of Mechanical Engineering, Cross River University of Technology, P.M.B 1123, Calabar, NIGERIA

²Energy, Exergy, and Environment Research Group (EEERG), Department of Mechanical Engineering, Michael Okpara University of Agriculture Umudike, P.M.B 7276, Umuahia, NIGERIA

³School of Design and Mechanical Engineering, Portsmouth University, UNITED KINGDOM

*Corresponding Author

Email: *johnevareh1234@gmail.com

Received 10 January 2020;
Accepted 25 February 2020;
Available online 20 March
2020

Abstract: This study focused on the computational design and static structural analysis of a small-scale turbojet engine (SSTE) that can power an unmanned aerial vehicle with a thrust of 50 N at a speed of 8000 rpm. SOLIDWORKS 2018 was used to design the CAD geometry of the SSTE, and to carry out a CFD analysis on the compressor to determine the pressure distribution across the compressor and the compressor pressure ratio. The obtained pressure ratio was further used to carry out a structural analysis of the SSTE with emphasis on the turbine component using ANSYS static structural module. This is because the turbine component is more susceptible to maximum stresses and temperature. However, this analysis was done to determine the level of deformation of the chosen design material (stainless steel grade 310), the maximum and minimum stresses, factor of safety, and its fatigue life. Design and CFD results obtained shows that the design is reliable as well as the pressure distribution in the compressor. The 50N small scale turbojet engine showed higher optimum performance from structural design and evaluation when compared to that of the 70N thrust jet cat model. Results of the structural analysis shows that the turbine blades will experience minimum and maximum deformation of 0 m and 2.2543×10^{-5} m at the leading edges and trailing edges of the blade chord respectively. Also, maximum and minimum stresses will occur at 1.0632×10^5 Pa and 6.7192×10^7 Pa respectively. Conversely, the factor of safety was within 3.0807 to 15 which show that the design is adequate. Additionally, considering the fatigue life, the SSTE is bound to fail completely at approximately 1.929×10^7 months. Therefore the SSTE with the materials suggested above is capable of propelling an unmanned aerial vehicle considering the results obtained.

Keywords: Computational, static-structural, turbojet, UAV, design

1. Introduction

The increased emphasis on faster unmanned aerial vehicles (UAVs) for command, control, communications, computers, intelligence, surveillance, and for weapon-delivery purposes raises some potential issues related to their propulsion systems [1][2]. Jet engines are most appropriate to solve this problem, but the system design and structural integrity becomes pertinent [2][3][4]. Aircraft engines and gas turbines wholly

work generally the same way by drawing a large volume of air via an inlet duct, compressing it before combustion with fuel, and then expanding the product of combustion through a turbine [5][6][7]. Therefore, five main components are required. These components include an inlet duct, a compressor, a combustion chamber, and a turbine (arranged in this exact sequence) with a driveshaft running through them [8]. A small turbojet engine is characterized by its thermodynamic cycle that describes the parameters of air and gas flow in cross sections, air flow rate, rotor's speed, fuel and its resulting

parameters such as specific fuel consumption and thrust [9]. Hitherto, traditional SSTE design study focused on model test and measurements alongside experiments which is not cost effective and a time saver [10]. [11] conducted a test on a Jetcat P-70 model jet engine. The study showed that the engine could produce a maximum thrust of 70N at a speed of 120,000 RPM, with an idle RPM of 35000. [12] also conducted a test on an AMT Olympus engine. It was discovered that the engine could produce a maximum thrust of 230N at a maximum speed of 112,000 RPM.

However, maximum thrust at a lower RPM and fuel consumption rate were not achievable by the models developed by [11][12], possibly as a result of the traditional design test process considered. Therefore, to achieve a more economic design, computational design methods using static structural analysis and computational fluid dynamics (CFD) analysis are introduced. These methods aim at improving SSTE designs and reducing apparent design stresses [13][14]. However, the amount of pressure or force the SSTE withstands to avoid failure decides its factor of safety [15]. The study objective is to recreate a 3D design geometry of a SSTE that can produce a Thrust of 50N for a speed as low as 8000 RPM and conduct a numerical analysis with the SSTE test rig conditions. Additionally, a static structural analysis is carried on the SSTE that produces higher thrust and lesser speeds than the models of [13][14], which make the propose model novel for consideration. This is necessary to determine the level of deformation of the chosen design material of the SSTE, the maximum and minimum stresses, factor of safety, and its fatigue life.

2. Structure

CAD model geometry of the SSTE was first developed followed by the compressor flow simulation to ascertain the pressure ratio and pressure distribution in the designed compressor. This however led to the Static Structural analysis of component materials.

2.1 Components description and materials selection

The mobile SSTE test rig depicted in Fig. 1 consist of a SSTE of 50N thrust mounted on a test bed. This SSTE is made up of a 5-stage axial flow compressor with improved blade aerodynamics, a compact size low pressure annular combustion chamber with good ignition behaviour and injection nozzles, and a single stage axial flow turbine with 37 blades of improved aerodynamics. It also has an electric motor attached to the shaft for start-up.

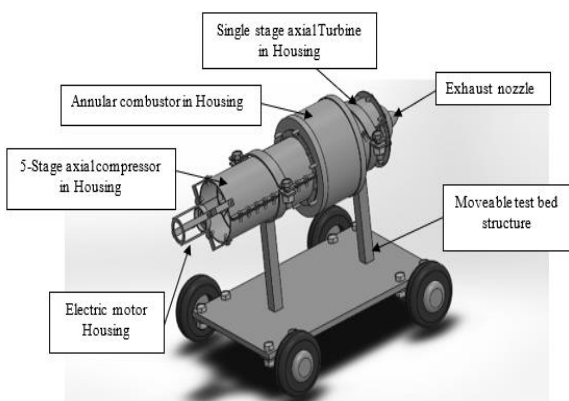


Fig. 1 – Experimental test rig of the SSTE

Turbojet materials includes titanium, nickel base alloys, composites, ceramics, aluminium, and steel [16]. However, materials used in constructing the 50N SSTE compressor, combustion chamber and turbine was stainless steel because of its ability to withstand temperatures up to 1150°C in continuous service and 1035°C in intermittent service, with a melting point range of 1400°C – 1450°C [17]. It is also corrosion resistant, ductile, of high strength and has an attractive appearance [16][17].

2.2 CAD Model Geometry Set up

Design and performance specifications were used to setup the model geometry and the simulation of the SSTE. However, assumptions that satisfy the turbojet design conditions were also made. Setting up the CAD interface for design was an important step in achieving the engine geometrical design objective. The SOLIDWORKS 2018 interface was accessed by launching the software using the program icon and selecting the parts design option that reveals the working interface. Design of different parts of the engine was carried out on this interface according to design specifications. After designing, parts were assembled in the assembly section of the CAD interface. Fig. 2 and Fig. 3 shows the translucent views of the designed SSTE geometry and the test rig, respectively.

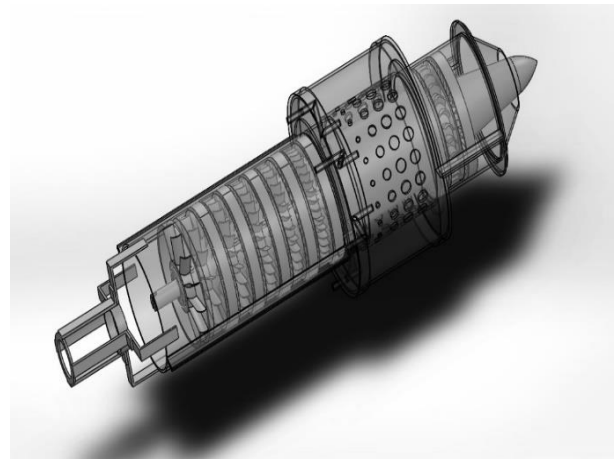


Fig. 2 – Translucent view of the designed SSTE geometry

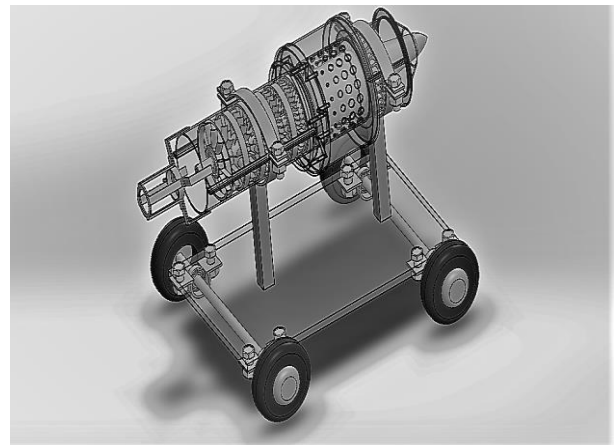


Fig. 3 - Translucent view of the designed SSTE test rig geometry

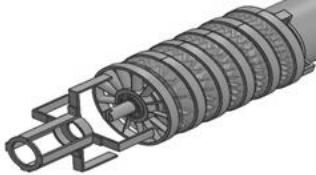



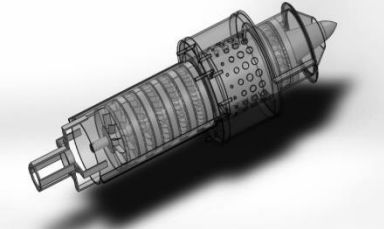
Performance specifications of the 50N SSTE used for the CAD geometry design process are presented in Table 1 and 2 while experimental assumptions made as retrieved from [11] are presented thus:

- Axial velocity (V_0) was constant through all stages.
- Combustion chamber efficiency, $\eta_{comb} = 0.95$
- Compressor inlet pressure, $P_1 = 101325\text{Pa}$
- Compressor inlet temperature, $T_1 = 15^\circ\text{C} = 288\text{K}$
- Fuel inlet velocity, $V_f = 48.23\text{m/s}$
- Gas constant, $R = 287\text{ kJ/kgK}$
- Nozzle efficiency, $\eta_n = 0.8$
- Nozzle pressure ratio, $\text{NPR} = 1.07$
- Required Thrust, $F = 50\text{N}$
- Number of revolutions per minute, $N = 8000\text{ rpm}$
- Specific heat ratio, $\gamma = 1.4$

Table 1 - Compressor stage performance and design parameters

Design parameters	Value
Speed, N (rpm)	8000
Rotational Speed, U (m/s)	36.86132267
Axial Speed, V_0 (m/s)	20.04313124
Whirl Velocity, V_{w1} (m/s)	16.81819142
Whirl Velocity, V_{w2} (m/s)	20.04313124
Relative Velocity V_{r1} (m/s)	28.34553987
Relative Velocity V_{r2} (m/s)	26.16596768
De Haller Number, $\frac{V_{r2}}{V_{r1}}$	0.92310705
Absolute Velocity, C_1 (m/s)	26.16596768
Absolute Velocity, C_2 (m/s)	28.34553987
Flow Coefficient, $\frac{V_0}{u}$	0.543744223
Stage Loading Coefficient, $\frac{\Delta H}{u^2}$	0.087488445
Compressor Stage Efficiency	77%

Table 2 SSTE performance parameters

Component	Schematics	Performance parameters	Values
Compressor		Compressor pressure ratio (from CFD simulation), r_p Compressor exit pressure, P_2 (Pa) Compressor exit temperature, T_2 (K) Work done by compressor, W_c (W) Compressor Isentropic efficiency, η_{ise} Inlet flow area, A_0 (m ²) Mass flow rate of air at compressor inlet, M_a (kg/s)	1.07 108417.75 293.6214999 5649.607386 0.9 0.00608 0.14189639
Combustor		Heat supplied, Q_{in} (W) Fuel mass flow rate, M_f (Kg/s) Fuel flow area, A_f (m ²) Fuel to air ratio, F_a	497038.72 0.0019 0.003926 0.013390052
Turbine		Turbine Entry Temperature, T_3 (K) Turbine entry pressure, P_3 (Pa) Turbine exit pressure, P_4 (Pa) Turbine exit temperature, T_4 (K) Work done by turbine, W_T (W)	788.1873905 291032.8552 271993.3226 679.8604014 108868.624
Nozzle		Nozzle exit velocity, V_e (m/s) Mass flow rate of gas at exit, M_e (kg/s) Nozzle exist area, A_e (m ²) Nozzle exit diameter, d_e (m) Nozzle exit Mach number, M_n	144.6721955 0.14379639 0.000187737 0.015460718 0.276802643
System performance		Net Thrust, NT (N) Net work done, W_{net} (J/s) Thermal efficiency, η_{th} Propulsive efficiency, η_p Specific fuel consumption, SFC (kg/Ns) Specific thrust, ST (Ns/kg) Engine Overall pressure ratio, OPR	50.01 103219.0166 0.207667959 0.243366925 0.000038 347.7138755 2.684365385

2.3 Computational fluid dynamics (CFD) setup

Flow simulation of the compressor was also carried out using SOLIDWORKS 2018 to ascertain the pressure distribution in the designed compressor and the compressor pressure ratio. The CFD interface for the flow simulation was activated and setup based on the type of simulation to be carried out. The wizard interface was opened and the name of the project, unit system, analysis type, type of fluid, type of fluid flow, fluid properties (pressure and temperature), and the flow coordinate system were set based on the test rig conditions (see Fig. 4). This setup opens the previous interface where the rotating regions, boundary conditions and the goals to be simulated were setup to run the simulation. The solver was set to use K- ω (SST) turbulence model and the Reynolds-Average Navier-Stokes (RANS) equation for the discretization and steady state solution. However, meshing of the design was automatically done by the SOLIDWORKS software while performing the simulation.

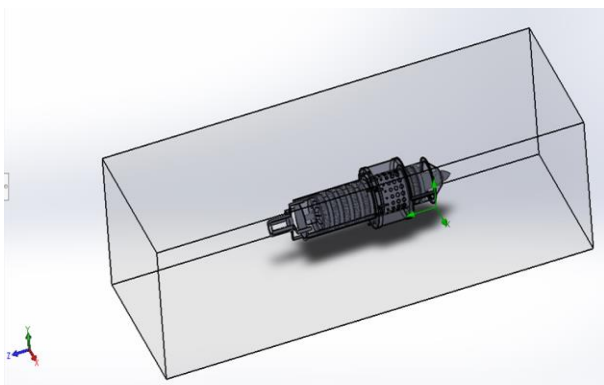


Fig. 4 – SOLIDWORKS flow simulation setup

SOLIDWORKS flow simulator was first used for the simulation of fluid flow in the compressor section of the engine. The parameters achieved from the compressor simulation formed the basis for the static structural analysis. Furthermore, the CFD setup is governed by some equation models represented in eqn. (1) to (4). These models consist of Reynolds-Averaged Continuity Equation, Reynolds-Averaged Navier-Stokes (RANS) equations, and K- ω (SST) turbulence model respectively.

CFD governing Equations

$$\frac{\partial \bar{u}}{\partial x} + \frac{\partial \bar{v}}{\partial y} = 0 \quad (1)$$

$$\rho \left(\bar{u} \frac{\partial \bar{u}}{\partial x} + \bar{v} \frac{\partial \bar{v}}{\partial y} \right) = -\frac{\partial \bar{p}}{\partial x} + \mu \nabla^2 \bar{u} + \bar{f}_{turb\ x} \quad (2)$$

$$\rho \left(\bar{u} \frac{\partial \bar{v}}{\partial x} + \bar{v} \frac{\partial \bar{v}}{\partial y} \right) = -\frac{\partial \bar{p}}{\partial y} + \mu \nabla^2 \bar{v} + \bar{f}_{turb\ y} \quad (3)$$

$$\frac{\mu_t}{\rho} \approx \frac{C_\mu k^2}{\epsilon} \quad (4)$$

Where,

Eqn. (1): Reynolds-Averaged Continuity Equation.

Eqn. (2) and (3): Reynolds-Averaged Navier-Stokes (RANS)

Eqn. (4): K- ω (SST) turbulence model

2.4 Static Structural Analysis Setup

The structural analysis was carried out using ANSYS STATIC STRUCTURAL V.19. This analysis was carried out to ascertain the level of deformation, maximum and minimum stresses and strain, factor of safety, and fatigue life of the SSTE

considering the material it was constructed with. Nonetheless, since the highest pressure and temperature of the engine occurs at the turbine component and its susceptibility to maximum thermal and mechanical stresses (Madhu 2016). The turbine was analysed and used as the criteria for validating the material usage. However, the turbine CAD design was imported into the ANSYS static structural geometry setup. The studied material was stainless steel grade 310, chosen from the ANSYS material library and has the following properties shown in Table 3. After the importation of the turbine CAD geometry and selection of material, the object was meshed into a suitable element size of 5×10^{-4} m for the analysis of the turbine. This element size gave a total number of 164,674 elements (cells) used in the analysis of this structure. Fig. 4 depicts the meshed object as well as the ANSYS static structural setup interface.

Table 3 - Properties of Stainless-Steel Grade 310 from ANSYS material library

Material Properties	Value
Density, (kg/m^3)	7750
Isotropic secant coefficient of thermal expansion, (C^{-1})	1.7×10^{-5}
Strength coefficient, (Pa)	1.66×10^9
Strength exponent	-0.15
Ductility coefficient	0.55
Ductility exponent	-0.55
Cyclic strength coefficient, (Pa)	1.96×10^9
Cyclic strain hardening exponent	0.28
Tensile yield strength, (Pa)	2.07×10^8
Compressive yield strength, (Pa)	2.07×10^8
Tensile ultimate strength, (Pa)	5.86×10^8
Young's Modulus, (Pa)	1.93×10^{11}
Poisson's ratio	0.31
Bulk Modulus, (Pa)	1.693×10^{11}
Shear Modulus, (Pa)	7.3664×10^{10}

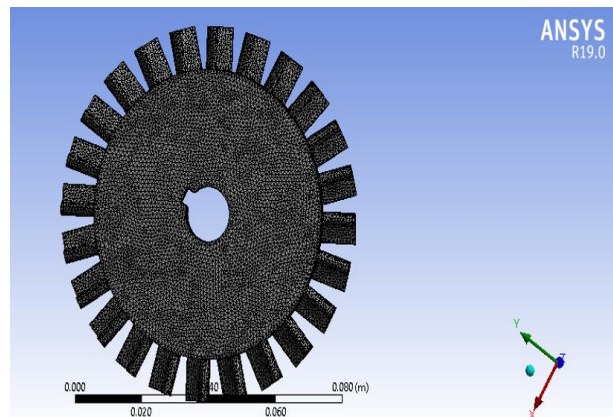


Fig. 4 - Meshed object and ANSYS structural interface

A fixed support was set on the body of the turbine, and the environmental temperature was setup to be 800°C. The temperature of the turbine at inlet was set at 800°C. The pressure acting on the turbine was also set to be 6×10^5 Pa in the Z-direction, and the rotational speed of the turbine was set at 800 rad/s. To obtain the fatigue life of the design, the strain life parameter was used assuming an infinite life of 1×10^{30} months and 1 cycle to be equivalent to 0.05 seconds which is equal to 1.929×10^{-8} months. The governing equations for the static structural analysis are presented in eqn. (5) to (15). These includes the FEA governing equations, 3D differential equations of equilibrium, constitutive model, and strain-displacement relations, respectively.

FEA governing equations

Force balance on infinitesimal element in x, y, and z directions.

Physical principle: Equilibrium of infinitesimal element

$$\vec{F} = m \vec{a} \text{ or } \sum \vec{F}_i = 0 \tag{5}$$

3D Differential Equations of Equilibrium

$$\frac{\partial \sigma_x}{\partial x} + \frac{\partial \tau_{xy}}{\partial y} + \frac{\partial \tau_{xz}}{\partial z} + f_x = 0 \tag{6}$$

$$\frac{\partial \tau_{xy}}{\partial x} + \frac{\partial \sigma_y}{\partial y} + \frac{\partial \tau_{yz}}{\partial z} + f_y = 0 \tag{7}$$

$$\frac{\partial \tau_{xz}}{\partial x} + \frac{\partial \tau_{yz}}{\partial y} + \frac{\partial \sigma_z}{\partial z} + f_z = 0 \tag{8}$$

Constitutive Model

$$\begin{bmatrix} \sigma_x \\ \sigma_y \\ \sigma_z \\ \tau_{yz} \\ \tau_{xz} \\ \tau_{xy} \end{bmatrix} = \frac{E}{(1+\nu) + (1-2\nu)} \begin{bmatrix} 1-\nu & \nu & \nu & 0 & 0 & 0 \\ \nu & 1-\nu & \nu & 0 & 0 & 0 \\ \nu & \nu & 1-\nu & 0 & 0 & 0 \\ 0 & 0 & 0 & 1-2\nu & 0 & 0 \\ 0 & 0 & 0 & 0 & 1-2\nu & 0 \\ 0 & 0 & 0 & 0 & 0 & 1-2\nu \end{bmatrix} \begin{bmatrix} \epsilon_x \\ \epsilon_y \\ \epsilon_z \\ \gamma_{yz} \\ \gamma_{xz} \\ \gamma_{xy} \end{bmatrix} - \frac{E}{1-2\nu} \begin{bmatrix} \alpha \Delta T \\ \alpha \Delta T \\ \alpha \Delta T \\ 0 \\ 0 \\ 0 \end{bmatrix} \tag{9}$$

Strain-displacement relations

$$\epsilon_x = \frac{\partial u}{\partial x} \tag{10}$$

$$\epsilon_y = \frac{\partial v}{\partial y} \tag{11}$$

$$\epsilon_z = \frac{\partial w}{\partial z} \tag{12}$$

$$\gamma_{xy} = \frac{\partial u}{\partial y} + \frac{\partial v}{\partial x} \tag{13}$$

$$\gamma_{yz} = \frac{\partial v}{\partial z} + \frac{\partial w}{\partial y} \tag{14}$$

$$\gamma_{xz} = \frac{\partial w}{\partial x} + \frac{\partial u}{\partial z} \tag{15}$$

3. Results and discussion

It is shown on Fig. 5 (showing the computational pressure flow distribution across the six stages of compression) that the air ingested into the compressor is at an ambient pressure of 101325 Pa and the pressure of air increases at each compression stage. However, the compressor exits pressure and pressure ratio obtained was 108417.75 Pa and 1.07 respectively as validated with the experimental. It is therefore established that the ingested air was compressed to increase the compressor exit pressure.

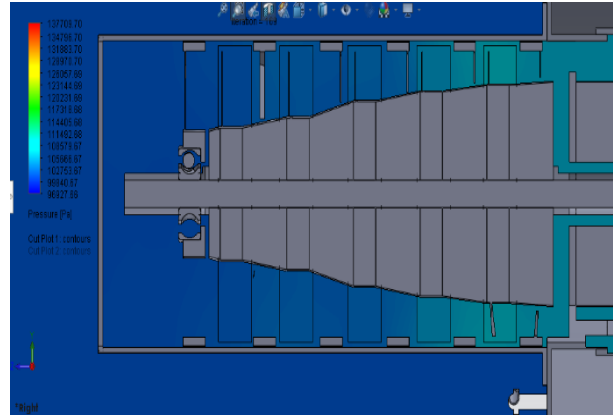


Fig. 5 - Pressure flow simulation of compressor section.

The results obtained from the static structural analysis of the turbine structure are categorized into five. This includes total deformation, equivalent elastic strain, equivalent stress, factory of safety, and fatigue life.

3.1 Total deformation

From the analysis it was discovered that when the SSTE is subjected to the setup conditions, there is a minimum and maximum deformation of 0 m and 2.2543×10^{-5} m respectively as shown in Fig. 6 and Fig. 7. The total maximum deformation occurs when the material completely fails. At this point the component is fully distorted and cannot function properly.

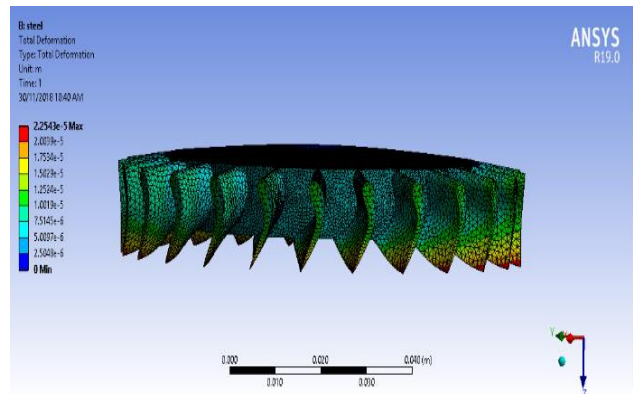


Fig. 6 - Side view of the total deformation that occurs on the turbine.

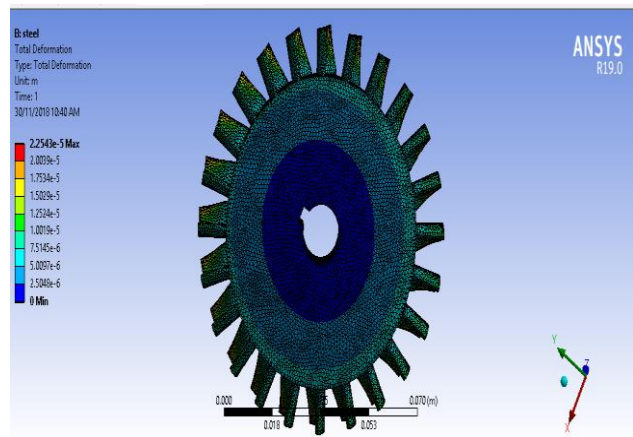


Fig. 7 - Front view of the total deformation that occurs on the turbine.

At the set-up condition, considering the blade chord, it is seen in Fig. 6 that the turbine blades will experience minimum and maximum deformation at the leading edges and trailing edges respectively. The susceptibility of the trailing edge of the turbine rotor blade to maximum deformation is as a result of its minimum thickness, presence of maximum pressures and vortices and to an extent, the angle of attack. From Fig. 7, the turbine component will experience minimum, intermediate, and maximum deformation at the root hub, blade disk, and blade tips respectively. The turbine blades tips are more susceptible to maximum deformation as a result of the total energy extracted by the turbine blades from the high enthalpy gases leaving the combustor. The blade root hub experiences minimum deformation because it is designed with maximum thickness.

3.2 Equivalent elastic strain

Fig. 8 and Fig. 9 depict that the minimum and maximum strain on the turbine is 1.3396×10^{-6} m/m and 4.0591×10^{-4} m/m respectively. The minimum strain experienced by the turbine at the leading edge of the blade chord is due to the total deformation that occurs at minimum stresses. While the maximum strain experienced at the blade chord trailing edges, blade root, root hub, and blade disk occur at maximum stresses. This is due to displacement of the material particles by the forces acting on the material, which leads to changes in the shape of the structure. Therefore, at the minimum strain deformation of the component starts to occur. While at maximum strain the turbine component is completely deformed and can no longer be used to achieve its purpose.

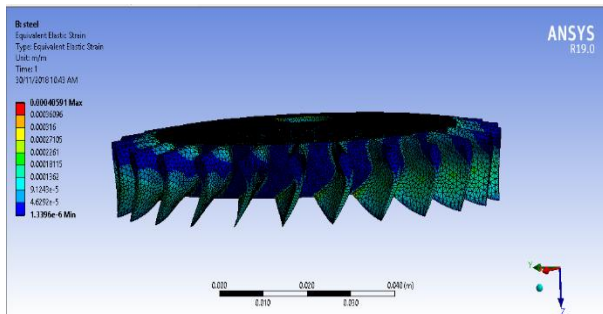


Fig. 8 - Side view of strain acting on the turbine.

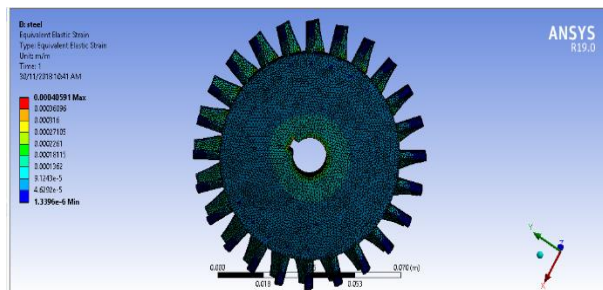


Fig. 9 - Front view of strain acting on the turbine.

3.3 Equivalent stress

The minimum and maximum stresses on the turbine are 1.0632×10^5 Pa and 6.7192×10^7 Pa respectively as shown in Fig. 10 and 11. The minimum and maximum stresses occur at the same relative part levels of equivalent elastic strain. The minimum stress value obtained is due to the pressure exerted on the turbine before deformation starts occurring. While the

maximum stress value obtained is the highest stress the turbine can withstand before complete deformation.

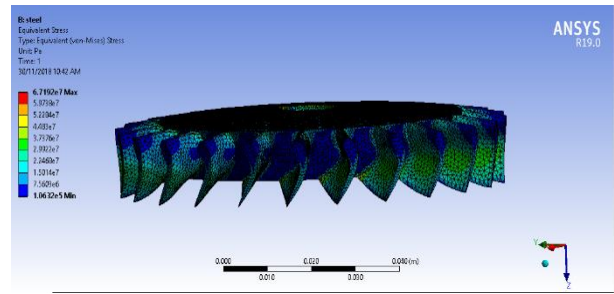


Fig. 10 - Side view of the stress acting on the turbine

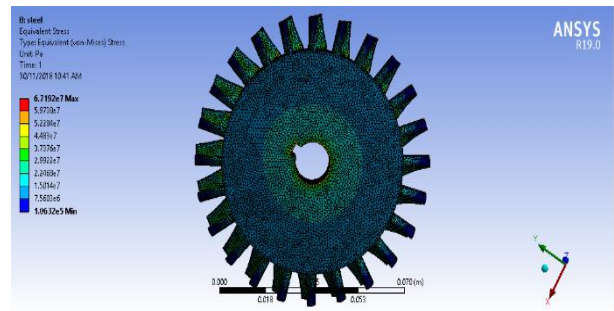


Fig. 11 - Front view of the stress acting on the turbine

3.4 Factor of safety

Fig. 12 and Fig. 13 illustrates that the factor of safety for the engine has a minimum and maximum value of 3.0807 and 15. Therefore the design is adequate. The minimum values indicate that for highly stressed areas, failure will occur at a load 3 times the applied pressure. While the maximum value shows that for areas with less stress concentration, the structure will fail at load 15 times the applied load.

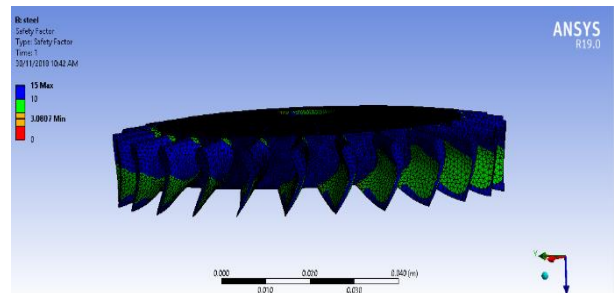


Fig. 12 - Side view of the factor of safety on the turbine.

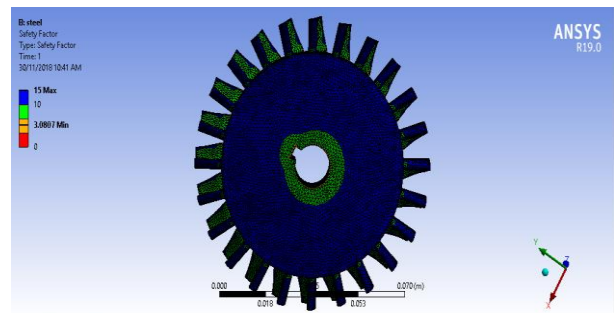


Fig. 13 - Front view of the factor of safety on the turbine.

3.5 Fatigue life

The fatigue life of the turbine is estimated at a minimum of 19.367 months and a maximum of 1.929×10^7 months as shown in Fig. 14 and Fig. 15, respectively. The minimum fatigue life shows how long the turbine will last before failure of any sort starts to occur; at this point the structure no longer functions effectively. While the maximum fatigue life shows how long the material will last before complete failure of the structure occurs.

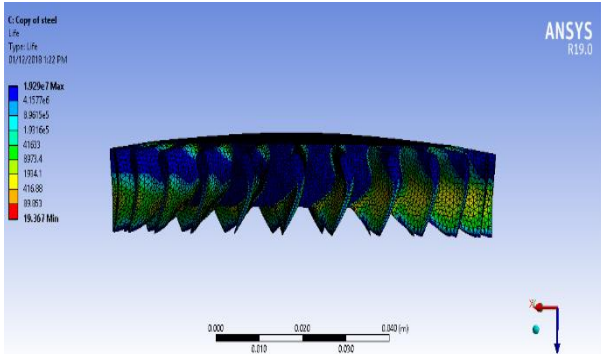


Fig. 14 - Side view of the fatigue life of the turbine.

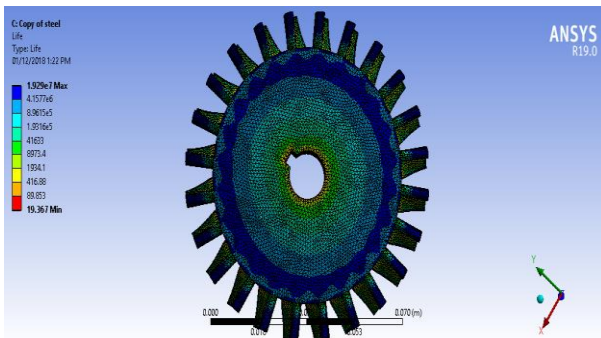


Fig. 15 - Front view of the fatigue life of the turbine.

4. Conclusion

The structural design and evaluation of a 50 N small-scale turbojet engine has been achieved. CFD analysis carried out on the compressor shows that the compressor produces a pressure ratio of 1.07 at the given speed of 8000 rpm as validated with experimental. Comparison of this analysis with that of [11] shows that the optimum performance of the designed engine is higher than the 70N thrust jetcat P-70 model jet engine that runs at a speed of 120,000 rpm, since greater thrust is achieved at a lower speed. Structural analysis conducted on the turbine component of the engine shows that, at the set up condition, minimum deformation, strain, stress, and factor of safety is obtained to be 0 m, 1.3396×10^{-6} m/m, 1.0632×10^5 Pa, and 3.0807 respectively. However, maximum deformations, strain, stress, and factor of safety is obtained to be 2.2543×10^{-5} m, 4.0591×10^{-4} m/m, 6.7192×10^7 Pa and 15. Therefore the design is adequate. The leading edge of the turbine blade chord, the blade disk and the turbine rotor hub are more susceptible to lower levels of stress, strain, and deformation. While the trailing edge of the turbine blade chord and the blade tips are more susceptible to higher levels of stress, strain, and deformation. Conversely, the fatigue life of the turbine is estimated at a minimum of 19.367 months and a maximum of 1.929×10^7 months. Therefore, putting these results into consideration, a conclusion can be drawn that the SSTE design is adequate considering stainless steel grade 310 material. Also, the 50 N thrust SSTE of 8000 rpm, 20.7% thermal efficiency,

24.3% propulsive efficiency, and 16 mm nozzle diameter can be used to propel UAVs.

References

- [1] M. Adamski, "Analysis of propulsion systems of unmanned aerial vehicles," *J. Mar. Eng. Technol.*, 2018, doi: 10.1080/20464177.2017.1383337.
- [2] M. Orkisz, P. Wygonik, and T. Wołoszyn, "PROSPECTIVE ALTERNATIVE PROPULSION SYSTEMS FOR UNMANNED AERIAL VEHICLES," *J. KONES. Powertrain Transp.*, 2014, doi: 10.5604/12314005.1130487.
- [3] S. N. Shivakumar, D. Chetan, P. Kumari, B. Sahana, and R. Mahalya, "Design and Analysis of Engine Mounting Frame of an Unmanned Aerial Vehicle," *Int. J. Res. Aeronaut. Mech. Eng.*, vol. 2, no. 5, pp. 27–35, 2014.
- [4] H. Ryaciotaki-Boussalis and D. Guillaume, "Computational and experimental design of a fixed-wing uav," in *Handbook of Unmanned Aerial Vehicles*, 2015.
- [5] S. O. Effiom, F. I. Abam, and B. N. Nwankwojike, "Performance evaluation of aeroderivative gas turbine models derived from a high bypass turbofan for industrial power generation," *Cogent Eng.*, 2017, doi: 10.1080/23311916.2017.1301235.
- [6] E. O. Samuel, F. I. Abam, and B. N. Nwankwojike, "Combined cycle performance evaluation of a simple and adapted aeroderivative gas turbines," *Niger. J. Technol. Res.*, 2018, doi: 10.4314/njtr.v13i2.6.
- [7] P. Singh Virdi, M. Saahil Khan, N. Pereira, S. K. V, and R. S. D, "Design and Fabrication of Major Components of Turbojet Engine," *Energy and Power*, 2017.
- [8] S. O. Effiom, F. I. Abam, and B. N. Nwankwojike, "Cycle parametric study on the performance of aeroderivative gas turbine models developed from a high bypass turbofan engine," *Cogent Eng.*, 2017, doi: 10.1080/23311916.2017.1368115.
- [9] R. Andoga, M. Komjáty, L. Fozo, and L. Madarász, "Design of the variable exhaust nozzle control system for a small turbojet engine MPM-20," 2014, doi: 10.1109/SAMI.2014.6822405.
- [10] G. J. J. Wessley and S. Chauhan, "Investigation on Scaling of Gas Turbine Engines for Drone Propulsion," *Int. J. Eng. Technol. Manag. Appl. Sci.*, vol. 5, no. 6, 2017.
- [11] J. E. Matsson, "Laboratory experience with a model jet turbine," 2004, doi: 10.18260/1-2--13003.
- [12] A. Horoufi and M. Boroomand, "Design and construction of microjet engine at amirkabir university of technology," 2009, doi: 10.2514/6.2009-4921.
- [13] T. T. Singh, J. S. Kumar, and D. Manish, *Flow Simulation & Static Structure Analysis (FEA) of a Radial Turbine*. 2015.
- [14] M. Odabae, M. Modir Shanechi, and K. Hooman, "CFD simulation and FE analysis of a high pressure ratio radial inflow turbine," 2014.
- [15] "Stress Analysis and Life Estimation of Gas Turbine Blisk for Different Materials of a Jet Engine," *Int. J. Sci. Res.*, 2016, doi: 10.21275/v5i6.nov164440.
- [16] B. W. Lagow, "Materials Selection in Gas Turbine Engine Design and the Role of Low Thermal Expansion Materials," *JOM*, 2016, doi: 10.1007/s11837-016-2071-2.
- [17] "New technology used in gas turbine blade materials," *Sci. Tech.*, 2007, doi: 10.22517/23447214.5037.